Titolo

Pre-test CFD analysis of the rod bundle experiment in the HLM facility NACIE-UP

Descrittori

Tipologia del documento: Rapporto Tecnico

Collocazione contrattuale: Accordo di programma ENEA-MSE su sicurezza nucleare e reattori di IV generazione

Argomenti trattati: Generation IV reactors
Tecnologia dei metalli liquidi

Sommario

At ENEA-Brasimone R.C., large experimental facilities exist to study HLM free, forced and mixed convection in loops and pools: e.g. NACIE-UP is a large scale LBE loop for mixed convection experiments. In the context of the SEARCH FP7 project, an experiment has to be performed in the NACIE-UP facility to assess the coolability of a 19-pin wire-wrapped electrical bundle (Fuel Pin Simulator, FPS), with heat flux up to 1 MW/m2. The bundle is representative of the one adopted in the MYRRHA concept.

The present paper is devoted to the Computational Fluid Dynamic (CFD) analysis of Heavy Liquid Metal (HLM) cooled Fuel Bundles to be adopted in the Gen-IV nuclear reactors.

A CFD analysis of fluid flow and heat transfer was carried out in the heavy liquid metal (LBE) cooled bundle test section of the NACIE-UP facility. The model includes the details of the wire-spacers as well as the entry region of the test section. A turbulence closure approach is adopted for all the simulations with ≈ 3.5·107 nodes and a resolution of y+ = 1

Note:

Autori:

R. Marinari, I. Di Piazza (ENEA)

Copia n. **In carico a: I. Di Piazza**

REV.	DESCRIZIONE	DATA		REDAZIONE	CONVALIDA	APPROVAZIONE
2			NOME			
			FIRMA			
1			NOME			
			FIRMA			
0	EMISSIONE	19/09/15	NOME	R. Marinari	M. Tarantino	M. Tarantino
			FIRMA			

Indice

1. Introduction

In the context of the studies on GEN. IV/ADS nuclear systems, the correct evaluations of the convective heat transfer in the core is of central interest. In particular, the use of Lead or Lead-Bismuth Eutectic (LBE) as coolant for the new generation fast reactors is one of the most promising choices.

Due to the high density and high conductivity of Lead or LBE, a detailed analysis of the thermo-fluid dynamic behavior of the Heavy Liquid Metal (HLM) inside the sub-channels of a fuel rod bundle is necessary in order to support the Front-End Engineering Design (FEED) of gen. IV/ADS fast spectrum demonstrative facilities like MYRRHA [1](Multi-purpose hybrid research reactor for high-tech applications). In this frame, the synergy between numerical analysis by CFD and data coming from large experimental facilities seems to be crucial to assess the feasibility of the components. At the ENEA-Brasimone Research Centre, large experimental facilities exist to study HLM free, forced mixed convection in loops and pools: i.e. CIRCE [2] is currently the largest experimental HLM pool facility in Europe and NACIE-UP is a large scale LBE loop for mixed convection [3].

The NACIE-UP experiment was designed in order to describe the thermal-hydraulic behavior of the MYRRHA FA during a Loss of Flow Accident (LOFA) with the coast-down of the main circulation pump.

The accident is protected loss of flow (PLOFA) if control rods can be inserted and the neutronic multiplication stops. In that case only the decay heat must be evacuated depending on the burn-up level, and at maximum 7% of the power should be considered in this case. Instead, the accident is unprotected (ULOFA) if the control rods cannot be inserted and the full power must be evacuated.

Heat transfer during a LOFA is driven by the inertia of the fluid during the pump coast-down and the onset of natural circulation due to the difference in height between the heat source and the heat sink. As a consequence of a LOFA, a stationary natural circulation flow rate will be established in a characteristic time which depends on the specific geometry of the system under consideration and on the geometry of the bundle.

To simulate the fuel pins, an electrically heated rod bundle was specifically designed and provided for this purpose.

The main difference between the MYRRHA bundle and the NACIE-UP bundle is the number of ranks and pins: 7 ranks and 127 pins for MYRRHA against 3 ranks and 19 pins for NACIE-UP. This difference in the number of pins is not relevant for the convective heat transfer in the sub-channels because side, corner and central sub-channels can be monitored in the 19 pin bundle and basic phenomenology is the same as in the MYRRHA bundle. For a fixed average velocity in the bundle, pressure drops are expected to be a little higher in the NACIE-UP bundle because the influence of the wall is stronger, but from the literature and from numerical evidences, it is clear that this difference is not really relevant [4]

A computational study was carried out on the experimental wire-wrapped bundle test section of NACIE-UP. The CFD model includes liquid metal and solid structures and it reproduces the real geometry of the section including the inlet and outlet regions. Wire-wrapped bundles

are widely investigated in the literature due to their dominant application in the sodium technology. Therefore, lot of works are present from the '60's to '80s when the interest for sodium technology was high [5-7]. In the last years, the interest in the liquid metal technology is high again due to the GEN. IV commitment and objectives: non-proliferation, economics, reduction of the long-life waste, safety, and higher efficient use of the fuel. With powerful modern computers, several numerical CFD studies appeared on the wire-wrapped bundles. For example, the Indian research is currently focused on the development of PFBR and LMFBR and try to develop numerical methodologies to analyze wire-wrapped configurations [8-10]. Numerical studies on wire-wrapped pin bundle cooled by heavy liquid metal are difficult to find in the literature.

1.1. Wire wrapped vs. grid spacer solution for the Fuel Assembly

The passage for the coolant flow between the fuel rods is maintained either by grid spacers or by thin wires wound around the rods. The prototype and demonstration plants in UK and Germany and the Fermi reactor in US used grid spacers; other plants use the wire-wrap spacer design. A steel wire of circular cross-section is welded at one axial extremity and spirally wound around the pin with a specified axial pitch.

Grid spacers, on the other hand, consist of a steel web structure anchored to the subassembly duct wall at specified axial levels. Less steel volume is occupied to provide a higher breeding ratio than wire wraps. In spite of this, wire wraps are preferred for several advantages. Firstly, they are easy to fabricate and less expensive. Further, mechanical vibration problems and reactivity oscillations are minimized by using wire wraps. This is because for every pitch of wire wrap, contact with adjacent cladding occurs at 6 axial locations.

To provide similar structural stability, grid spacers require several grids, resulting in excessive pressure drop. The wire-wrap design also enables better thermal mixing of coolant due to induction of lateral velocity components and increase in local turbulence level.

2. The NACIE-UP experimental loop

2.1 General framework

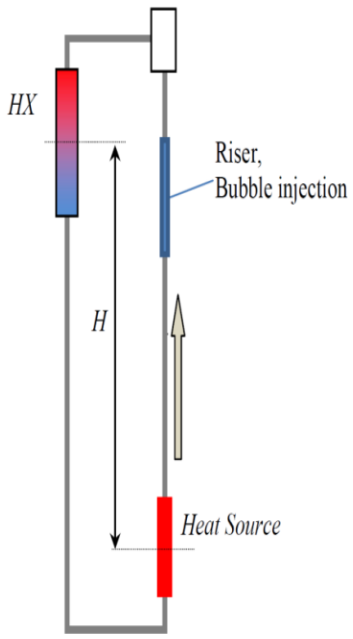

Figure 1 Conceptual sketch of the NACIE-UP

A schematic layout of the primary loop is reported in Figure 1. The reference for the piping and instrumentation is the P&ID reported in Figure 2, where all the instrumentation, components and pipes are listed and logically represented. The facility includes:

- The Primary side, filled with LBE, with 2 ½" SS AISI304 pipes, where the main new components and instruments will be placed:
- A new Fuel Pin Simulator (19-pins) 250 kW maximum power;
- A new Shell and tube HX with two sections, operating at low power (5-50 kW) and high power (50-250 kW);
- A new low mass flow rate induction flow meter (0-3 kg/s) FM101;

- A new high mass flow rate induction flow meter (3-15 kg/s) FM102;
- 5 bubble tubes to measure the pressure drops across the main components and the pipes;
- Several bulk thermocouples to monitor the temperature along the flow path in the loop;
- The Secondary side, filled with water at 16 bar, connected to the HX, shell side. It includes a pump, an air-cooler, by-pass and isolation valves, and a pressurizer (S201) with cover gas;
- An ancillary gas system, to ensure a proper cover gas in the expansion tank and to provide gas-lift enhanced circulation;
- A LBE draining section, with ½″ pipes, isolation valves and a storage tank (S300);
- A gas-lift circulation system in the riser ensures about 0.6 bar of driving force.

The LBE melting temperature is about 130 °C; therefore, the typical operating temperatures in the loop are above 200 °C. The difference in height between the heating section and the Heat exchanger is about 5 m to perform natural circulation tests. Due to the high LBE density (≈10300 kg/m^3), the hydrostatic pressure gradient in the facility is around 1 bar/m.

2.2 The experimental bundle test section

The FPS will consist of 19 electrical pins with an active length L_{active} = 600 mm. The whole length (L_{total} = 2000 mm) includes the non-active length and the electrical connectors. The pin has a diameter D = 6.55 mm, and the maximum wall heat flux will be close to 1 MW/m^2. The pins are placed on a hexagonal lattice by a suitable wrapper, while spacer grids will be avoided thanks to the wire spacer. The total power of the fuel pin bundle is ~ 235 kW.

This fuel pin bundle configuration is relevant for the MYRRHA's core thermal-hydraulic design [1].

The goals of the experimental campaigns planned on the NACIE-UP facility with the new bundle are: the measurement of the pin cladding temperature by embedded thermocouples; the measurement of the sub-channels temperature; Heat Transfer Coefficient (HTC) evaluation; the check of hot spots and peak temperatures; the evaluation of the axial thermal stratification entrance length along the sub-channels.

A schematic representation of the cross-section of the pin bundle is shown in Figure 3. The total flow area can be conventionally divided into 54 sub-channels of different ranks (S1-S54). The sub-channels and the relative pins that will be instrumented are also indicated in Figure 3. Wires are helicoidally twisted around each pin.

The main geometrical dimensions to be considered for a thermal-hydraulic assessment of the FA are:

- The rod diameter D=6.55 mm;
- The wire diameter d=1.75 mm;
- The pitch to diameter ratio P/D =1.2824;
- The streamwise wire pitch Pw=262 mm;
- The regular lattice is triangular/hexagonal staggered;
- The resulting flat to flat distance of the hexagonal wrap is 39.34 mm;
- The equivalent hydraulic diameter of the bundle is D_{eq}=4.147 mm;

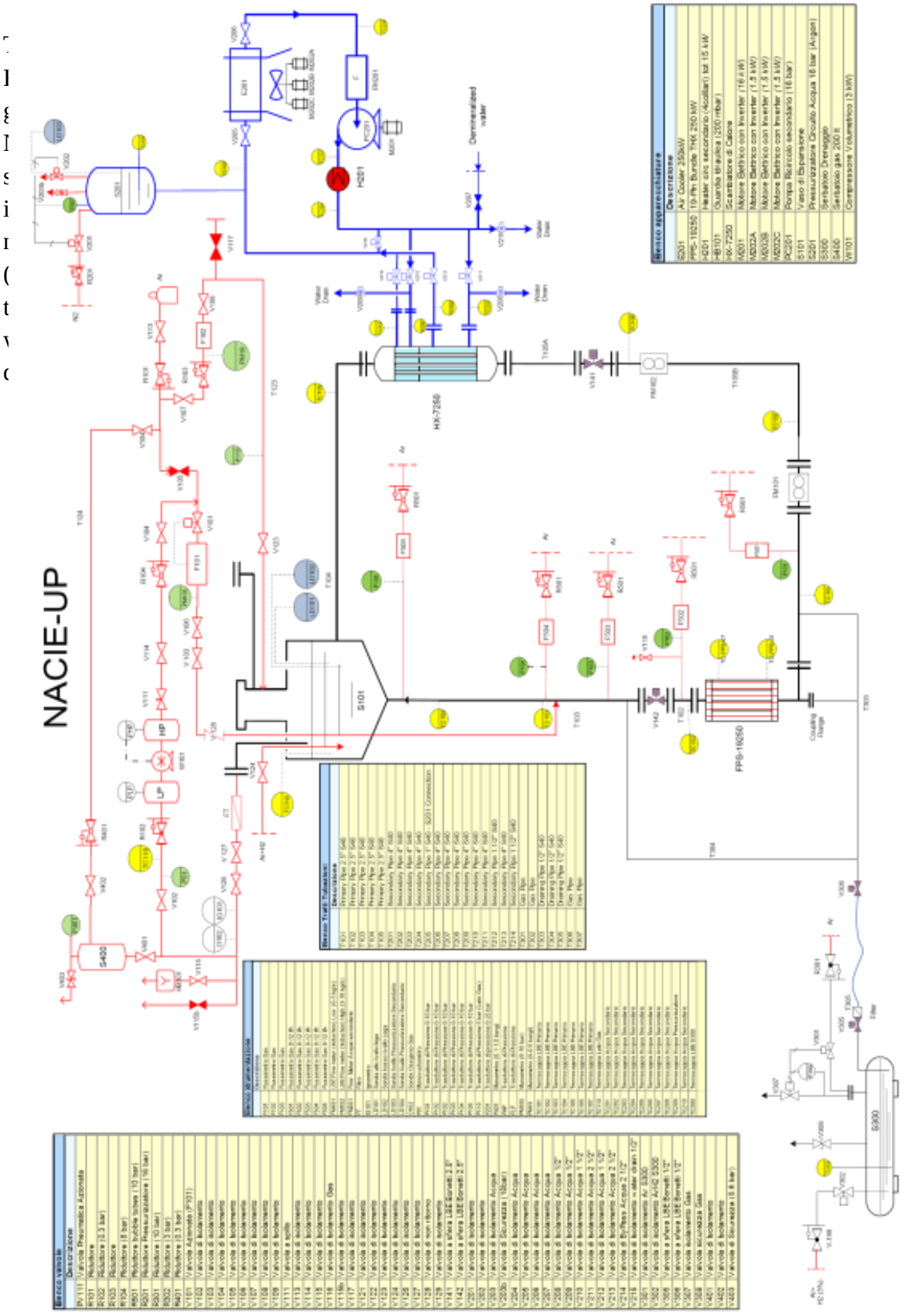

Figure 2 Piping and Instrumentation Diagram (P&ID) of the NACIE-UP facility.

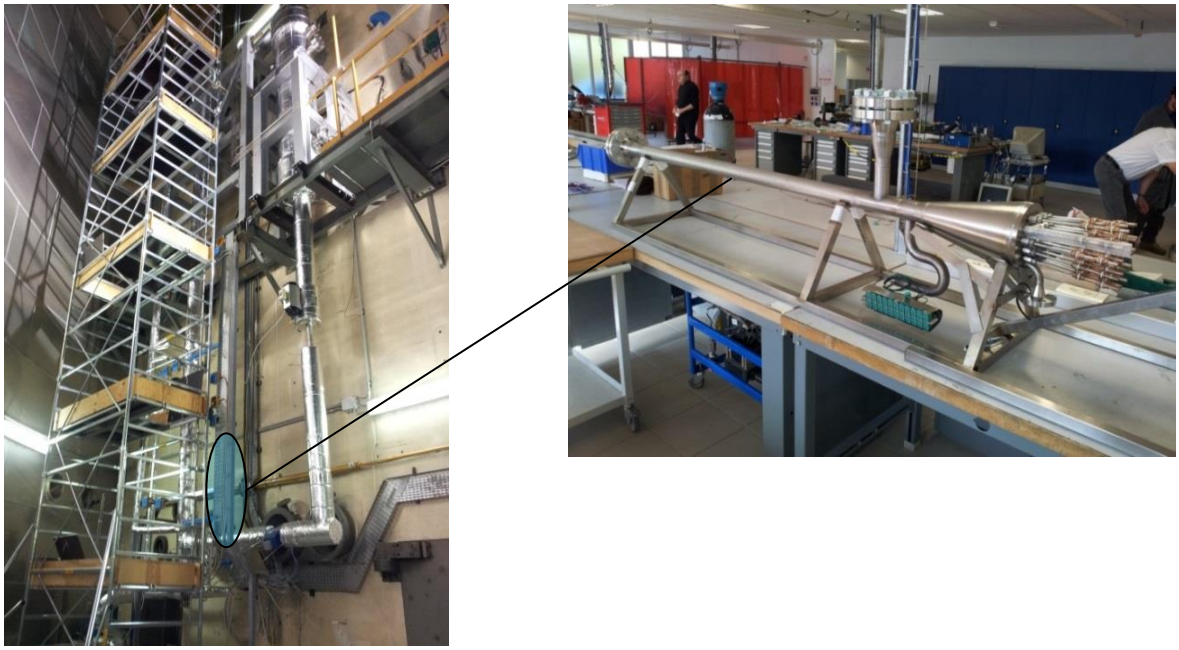

Figure 4 The NACIE-UP facility with an highlight of the FPS and its location

3. Code Assessment

As a preparatory step to the CFD pre-test analysis of the NACIE-UP test section, it is necessary to validate the ANSYS CFX code and the numerical approach for the wire-wrapped bundle geometry. As it was expected, in the literature there is a lack of experimental data on lead or LBE cooled wire-wrapped bundle. For this reason, the sodium cooled wire-wrap pin bundle designed and tested by M.H. Fontana et al. [11]. at ORNL was chosen as reference experimental data set. The geometry of the bundle and the Reynolds number range are both very similar to the NACIE-UP FPS. The working fluid is different, i.e. sodium with a Prandtl number around 0.005 lower than LBE.

The Fuel Failure Mockup (FFM) is a sodium test facility built specifically for testing simulated LMFBR core segments at Fast Test Reactor (FTR) design power and coolant flow conditions.

The FFM is a large, high-temperature sodium facility in which 19-pin bundles simulating LMFBR core segments were subjected to thermal-hydraulic testing at FTR conditions. The core segments are simulated by electric cartridge heaters duplicating reactor fuel pin configuration and heat flux. Spirally wrapped wire-like spacers containing both grounded and ungrounded thermocouple junctions space the heaters in the assemblies.

A number of heater bundles were scheduled to be tested in the FFM.

Bundle 2A (simulated in this study), consisted of 19 pin bundle with wire spacers and the rod diameter (5.84 mm), the pitch to diameter ratio (1.24), the wire pitch (305 mm) and the length of the active region (533 mm) are very similar to the NACIE-UP test section as shown in Table 1.

Table 1 Comparison between the geometrical parameters of the Fontana Bundle 2A and the test section of the NACIE-UP facility.

	Fontana Bundle 2A	NACIE-UP Test section
Rod diameter [mm]	5.84	6.55
Pitch to diameter ratio	1.24	1.28
Wire pitch [mm]	305	262
Length of the active region [mm]	533.75	600
Working Fluid	Sodium	LBE

3.1 The CFD model

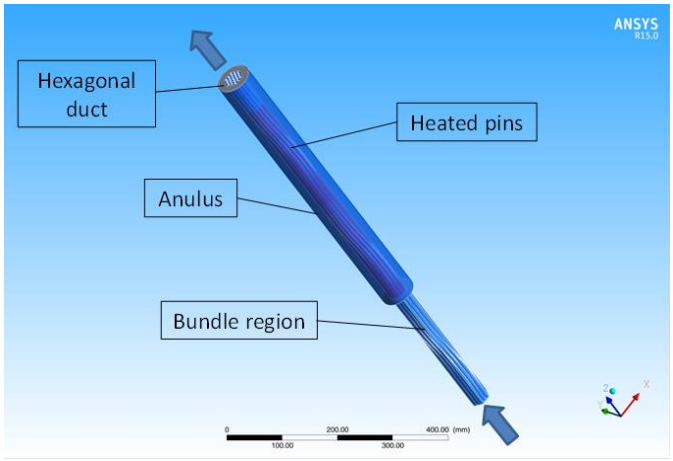

Figure 5 Layout of the CFD model developed for the bundle 2A.

The model developed includes the entire pin bundle length with the preceding and follower unheated regions and the heated one. The hexagonal duct is included into the model with the small annular fluid region between the test section housing and the pin bundle simulator for heat transfer reasons. The length of the hexagonal duct as the one of the annular region cover the heated region and the follower unheated one (because thermocouples are installed also there). A sketch of the model developed can be seen in Figure 5.

The wire spacer is modeled with the interference solution already adopted for the NACIE-UP bundle. The annular region as well as the hexagonal duct are included to describe the conjugate heat transfer and to correctly describe the boundary conditions.

For the fluid into the pin bundle an unstructured tetrahedral mesh was adopted; the number of elements was increased near the solid structures achieving a $y^+ \sim 1$ at the higher Reynolds number simulated. In the annular fluid region, a really fine structured mesh and an high resolution of the viscous sub-layer ($y^+ \sim 1$) was adopted. The hexagonal duct exploits a semi-structured mesh method.

The working fluid simulated is Sodium with constant properties fixed at 340 °C. Every buoyancy effect is neglected ($Ri_{tr} \ll 1$ in every simulation performed).

All the simulations are stationary RANS, the turbulence model adopted is the k-ω SST model. The mass flow rate and the inlet temperature were imposed at the fluid inlet sections (both for bundle region and annular region). A constant zero pressure was kept on both outlet sections. A constant heat flux condition was imposed on the external surface of the annular region and on external hexagonal surfaces of the bundle inlet region (with not heated pins) because, during the tests, the outside heating cables were kept on; the total power imposed to simulate the heating cable power was derived from the declared data. A constant heat flux condition, specific for every pin, was imposed on pins' surfaces according to the test data.

For a better assessment of the ANSYS CFX code with wire wrapped geometry, the lower sub-channel Reynolds number cases were selected (more similar to the NACIE-UP test matrix cases).

3.2 Results

For sake of simplicity only one simulation is reported in this summary.

- **TEST SERIES 4, RUN 105 :** the main data of this test are reported in Table 2.

Table 2 Operating data of TEST SERIES 4 RUN 105 case.

$\dot{m}_{total}$ [kg/s]	$\dot{m}_{anular}$ [kg/s]	Re [-]	W_{pins} [kW]	W_{cables} [kW]	T_{inlet} [K]
0.27	0.013	8380	31.13	5.95	587

The CFD results are compared with temperatures measured near pins and walls by ungrounded thermocouples at different heights. Figure 7 shows that the temperature difference between CFD results and experimental values could reach 13.6 K. More accurate predictions could be reached for the duct (internal wrap) wall temperatures as we can see in Figure 6, where the maximum temperature difference is 9.9 K (at the entrance of the heated region where the thermal field is not developed), while the mean difference is 3.4 K. The different agreement shown in the two comparisons is justified by the absence of the solid structures of the pins in the CFX model and an inaccurate description by the authors of thermocouples position and the pin bundle

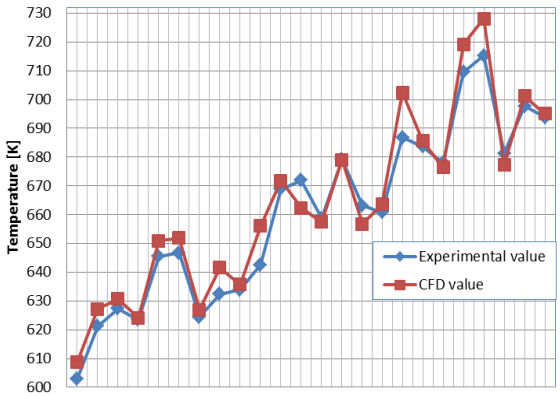

Figure 7 Comparison of pin temperature predictions at different heights with TEST SERIES 4-RUN105 experimental results

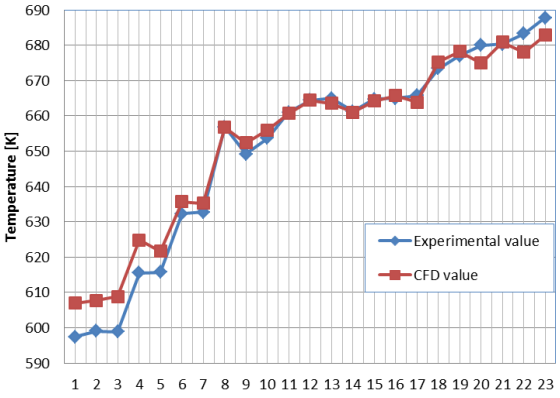

Figure 6 Comparison of duct (wrap internal) temperature predictions at different heights with TEST SERIES 4-RUN105 experimental results

geometry.

The CFD model results have a good but not excellent agreement with the experimental data especially in the central region of the bundle. This not perfect agreement can be explained by the inaccurate description given by the authors of the pin bundle geometry, the considerable thermal gradient across the wire-wrap spacer and the unspecified exact position of the wire-wrap thermocouples. On the overall, CFD code assessment can be considered acceptable.

4. The CFD model of the FPS bundle

A CFD analysis was performed on the pin bundle test section as pre-test of the experimental campaign. A technical drawing of the test section is reported in Figure 8.

The whole FPS test section was modelled including the inlet region, the entry region, the active region, the outlet region with the upper grid, and the hexagonal wrap, see Figure 9. The exact geometry of the pins with wire was also reproduced by collapsing the wire into the pin clad by a small surface contact, see detailed mesh view in Figure 9. This practice allows better mesh generation on the fluid side and it is commonly used in the literature, see for example [10].

The model shown in Figure 9 includes the conjugate heat transfer in the pin clad, in the wire and into the hexagonal wrap. It should be stressed that the hexagonal wrap in the experimental test section is obtained from a stainless steel full rod by electrochemical erosion; this implies that the wrap is very thick and the conjugate heat transfer effects may be relevant.

Regarding the mesh generation strategy, the inflation was used close to solid-fluid interfaces on the fluid side (structured hexahedral elements). This choice guarantees good mesh properties close to the wall and it implies a better numerical discretization for the wall phenomena. In the bulk of the fluid, the unstructured mesh was adopted. In the solid domains, an hexahedral dominant mesh was used. The total number of nodes and elements in the model are $3.5 \cdot 10^7$ and $9.7 \cdot 10^7$ respectively.

The simulations were performed by using ANSYS-CFX 15 [12] with the Shear Stress Transport (SST) k-ω turbulence model [13] and a second-order scheme for convective terms. The turbulent Prandtl number has been set to 1.5, as suggested by several studies on heat transfer in heavy liquid metals at moderate Peclet numbers [14].

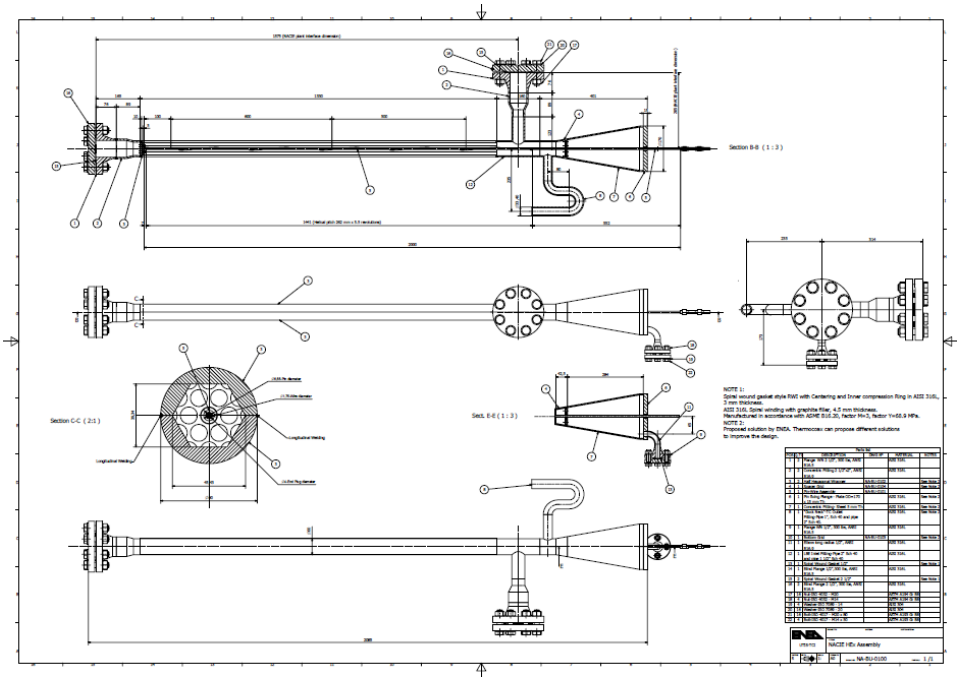

Figure 8 Overall bundle layout: technical drawing

A total mass flow rate ($\dot{m} = 0.5 - 7\,kg/s$), constant temperature (T_{inlet}=200 $°C$), boundary conditions were imposed at the inlet coherently with the test matrix of the experimental campaign, while pressure boundary conditions were imposed at the outlet. At the internal pin wall in the active region, a constant heat flux q'' was imposed. The computational mesh

adopts a resolution close to the wall such to achieve a y^+ of the order of 1 for 2 *kg/s* and of the order of 4 for 7 *kg/s*. These features guarantee high accuracy to the model, minimize the discretization error and allow to integrate turbulence model equations down to the viscous sublayer.

Constant thermo-physical properties were assumed for LBE at 250°C, according to Table 3

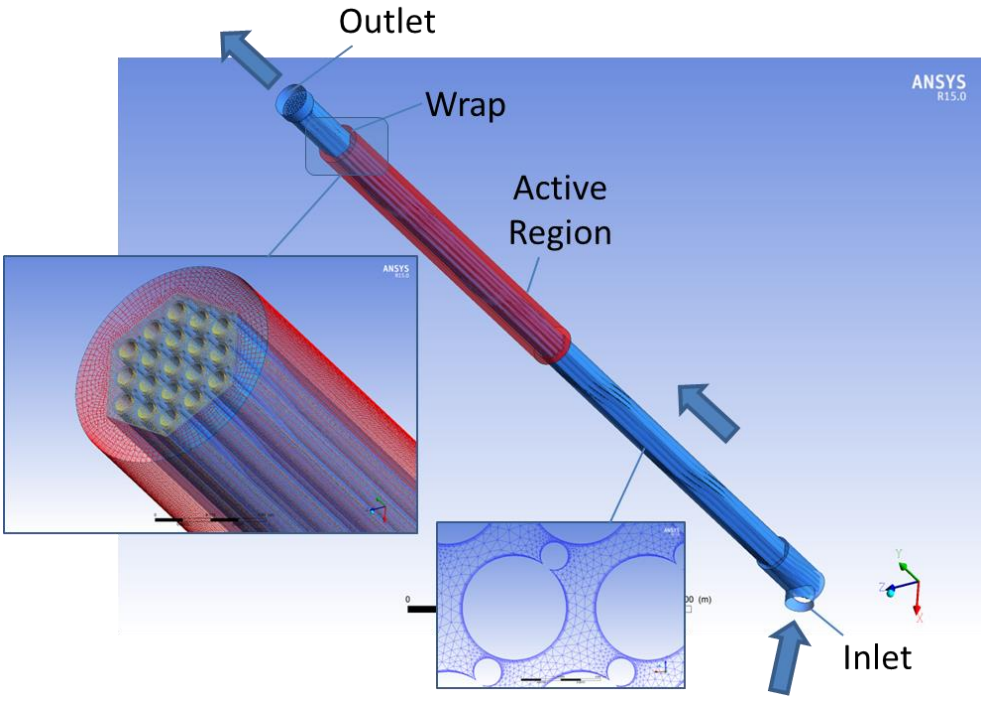

Figure 9 NACIE-UP CFD model layout with details of computational mesh

[15]. For the clad, wrap and wire material (SS AISI 304), constant physical properties were considered at 250 °C.

Table 3 Physical properties of LBE at 250 °C.

ρ [kg/m^3]	Density	10403
ν [m^2/s]	Kinematic viscosity	$2.007 \cdot 10^{-7}$
k [$W/(m\ K)$]	Thermal conductivity	11.34
c_p [$J/(kg\ K)$]	Specific heat at constant pressure	146.7
Pr [-]	Prandtl number	0.0259

5. Sensitivity analysis

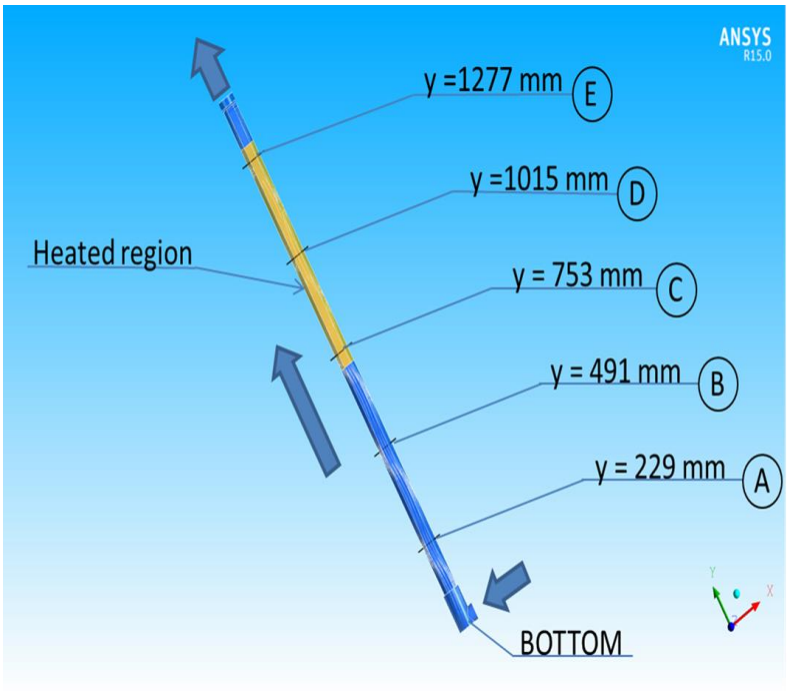

Figure 10 Detailed representation of the cross-section planes with their nomenclature and their height from the BOTTOM

Different sensitivity analyses were carried out to fix the CFD model of the NACIE-UP pin bundle.

For a correct sensitivity analysis and a detailed analysis of the CFD results, different cross-section planes were adopted, one wire pitch (262 mm) far one from the other. In Figure 10 the position of the planes is reported by indicating the distance from the BOTTOM plane and the nomenclature adopted in the next paragraphs. It has to be pointed out that there are three cross-section planes into the heated region (in **orange**), at the same heights of the FPS thermocouples, i.e. actually coincident with the measuring planes.

All the sensitivity analyses reported here (except where specifically described) adopted a specific reference case with an inlet mass flow rate of 2.032 kg/s, a sub-channel Reynolds number of 6162 and a total thermal power of 32.52 kW uniformly distributed in the heated length; the same data are reported in Table 4. The case is in the transitional region and at the center of the NACIE-UP experimental test matrix.

Table 4 Data setting of the reference case studied in the sensitivity analysis.

$\dot{m}_{NACIE}$ [kg/s]	u_{sc} [m/s]	Re_{sc} [-]	Thermal power [kW]
2.032	0.29	6162	32.52

5.1 The influence of mesh size

Three different meshes were developed on the fluid domain:

- ✓ a coarse mesh ‘C’ with 10 million total nodes;
- ✓ a medium mesh ‘M’ with ~ 22 million nodes;
- ✓ a fine mesh ‘F’ with ~ 29 million nodes.

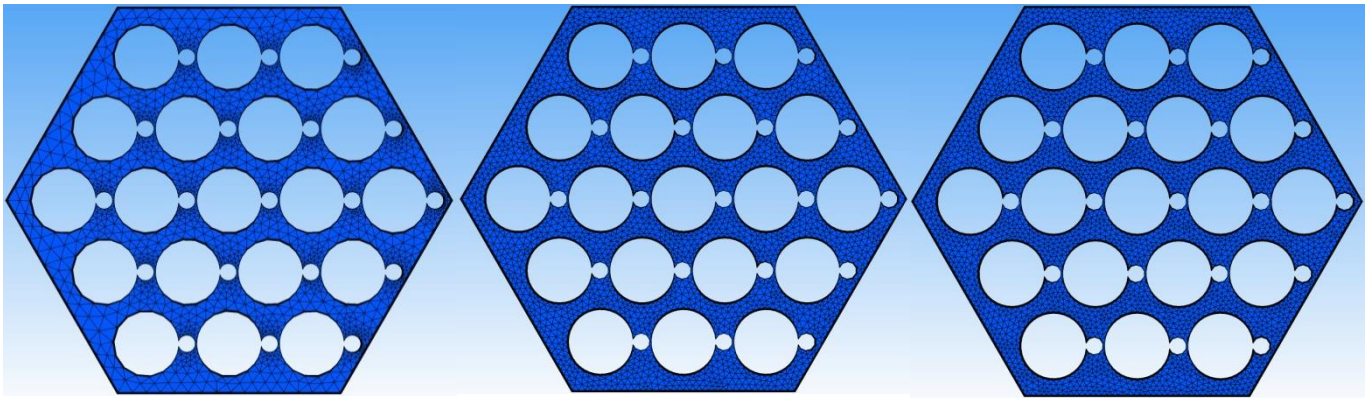

Figure 11 Cross sections of the grain size for the coarse mesh (left), the medium mesh (center) and fine mesh (right).

The grain size of the three meshes is shown in Figure 11; all the meshes have a resolution of y^+~1 at the wall with inflation for the reference case.
Comparison was performed on the reference case on the following fields: mainstream axial velocity, secondary velocity, temperature.

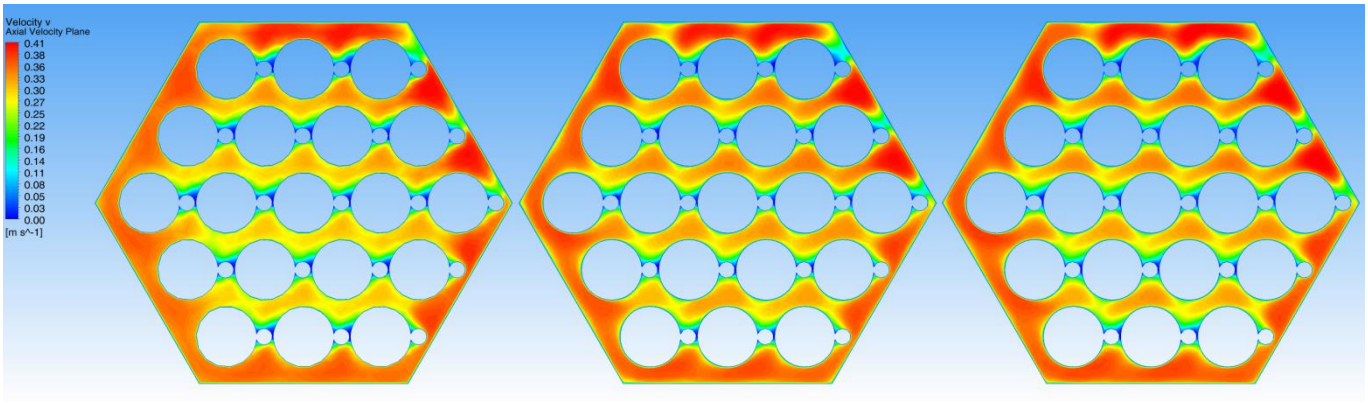

Figure 12 Axial velocity profiles at the middle of the active zone for : coarse size mesh (left), medium size mesh (center) and fine size mesh (right).

The axial velocity profile at the middle of the active region, is reported in Figure 12.
There are not significant differences between the medium size mesh M and the fine size mesh F, while the coarse size mesh C under-predicts the mainstream velocity in the interior sub-channels of the bundle.
Another interesting comparison takes into account the swirl (secondary) velocity field on the same cross-section of the previous comparison (Figure 13). The swirl velocity is here defined

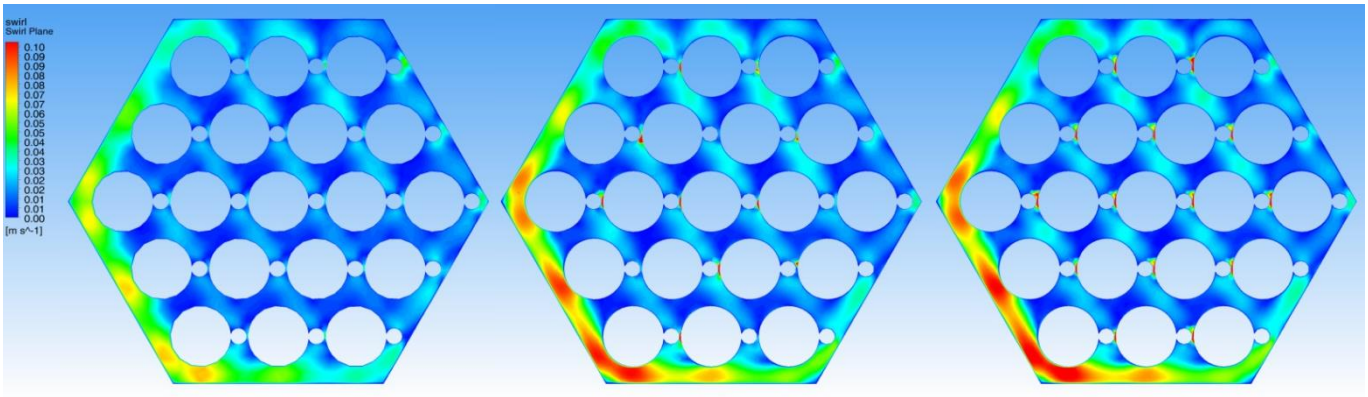

Figure 13 Swirl velocity profiles at the middle of the active zone for : coarse size mesh (left), medium size mesh (center) and fine size mesh (right).

as the magnitude of the component of the velocity vector orthogonal to the mainstream direction, i.e. in the plane of the cross-section. From the comparison, it is possible to notice again that the coarse size mesh C under-predicts the magnitude of the swirl velocity component even if it's able to predict the maxima locations. The medium (M) and fine size (F) meshes, on the other hand, give practically the same results.
Looking at the thermal field, the temperature contours on the same plane of the previous comparisons are extrapolated for the three cases and reported in Figure 14. The same

conclusions of the previous cases could be depicted, with a substantial grid independence of the quantity.

As a conclusion of the mesh independence study, the medium size mesh was chosen for the subsequent sensitivity studies and test-matrix simulations.

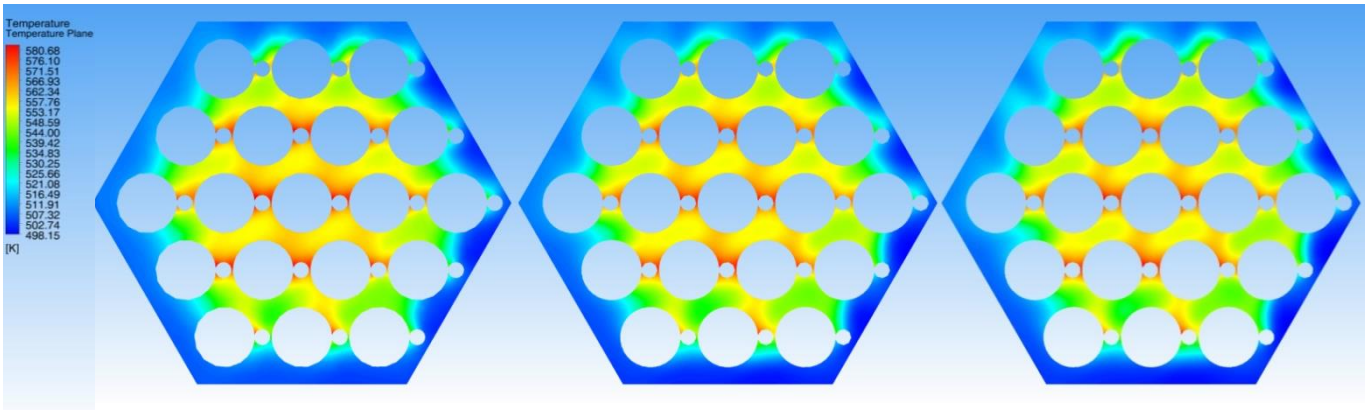

Figure 14 Temperature profiles at the middle of the active zone for : coarse size mesh (left), medium size mesh (center) and fine size mesh (right).

5.2 The influence of solid structures

The inclusion of the solid structures into the CFD model was developed for taking into account the conjugate heat transfer effect of the outward hexagonal wrap. In particular the hexagonal wrap has a considerable thickness due to the specific mechanical construction derived from a full SS pipe by a milling cutter. Therefore low resistance solid region thermal 'bridges' exist between hot and cold outwards regions of the LBE. Pins and wires were also modelled and meshed with at least one node into the pin clad, for a more realistic simulation of the heat transfer phenomena between the solid pins and the fluid LBE.

Figure 15 shows the temperature contours in section D for the model without solid structure (left) and with solid structures (right). The conjugate heat transfer effect of the outward hexagonal pipe causes a more uniform temperature distribution in the external sub-channels of the pin bundle, smoothing the cold regions in the lower-right part of the cross-section.

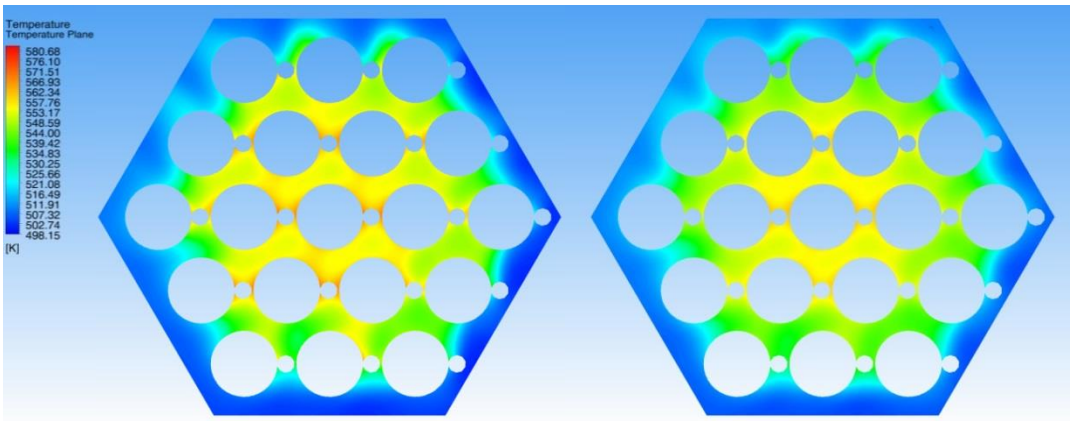

Figure 15 Comparison of temperature contours on the same cross-section for the preliminary

Local temperature differences in the same points between the two models can be 10-15 °C or more. All these phenomena cannot be neglected and allow to assess that for a reliable

simulation of the NACIE-UP pin bundle thermal field, the outward pipe structures must be included into the CFD model to describe the conjugate heat transfer.
From the same comparison, the pins' modelling effect on the thermal field can be deduced; the residual hot-spots in the small gaps between the wire spacers and the pins adjacent to it tend to disappear thanks to the smoothing effect of the heat transfer between the pin and the wire and through the wire from one side of the fluid to another.

6. Pre-test analysis

For the pre-test analysis of the NACIE-UP pin bundle, a specifically numerical test matrix was developed with mass flow rates ranging from 0.5 kg/s to 7 kg/s, according to the gas lift system capabilities and the experimental test matrix, and heating power inputs imposed for having an inlet-outlet temperature difference of 110 °C (as in the experimental test matrix). The numerical test matrix is doubled because the same cases are simulated either with the preliminary model (only fluid -OF-) and with the complete model (with solid structures -SS- included) . The test matrix is reported in Table 5.

Table 5 Numerical test matrix developed for the pre-test analysis of the NACIE-UP pin bundle; the average sub-channel velocity u_{sc} , the Reynolds number and the Peclet number are also reported.

Preliminary model cases	Complete model cases	$\dot{m}_{NACIE}$ [kg/s]	Power [kW]	$\bar{u}_{sc}$ [m/s]	Re_{sc}	Pe_{sc}
OF05	SS05	0.5	8.07	0.07	1516	41.0
OF10	SS10	1.0	16.14	0.15	3032	82.0
OF20	SS20	2.032	32.52	0.29	6162	166.5
OF30	SS30	3.0	48.42	0.44	9097	245.8
OF40	SS40	4.0	64.56	0.58	12130	327.7
OF50	SS50	5.0	80.70	0.73	15162	409.6
OF60	SS60	6.0	96.84	0.88	18195	491.5
OF70	SS70	7.0	112.97	1.03	21227	573.5

For sake of simplicity, only the analysis of the transitional flow regime case (SS20 and OF20) will be described because the other cases studied show similar behaviors.
Figure 16 reports the development of the axial velocity component on the five cross-section planes, all the contours have the same scale reported in the upper left corner for completeness;

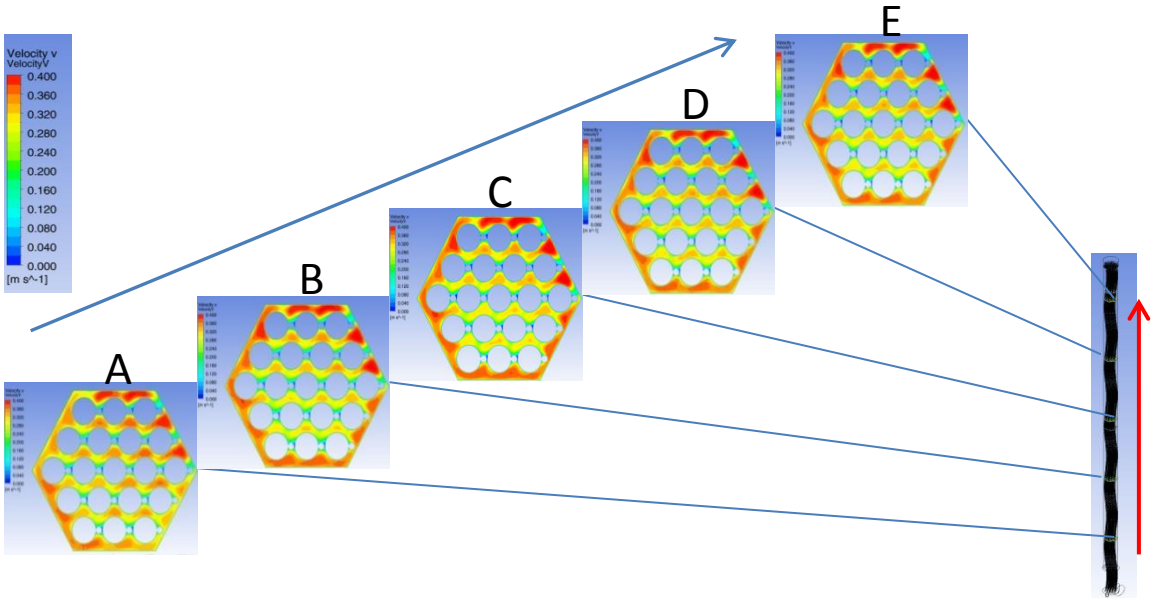

Figure 16 Development of the mainstream velocity component for the 2.032 kg/s case.

the axial component is already developed well before the heated region, and it's fully developed after two wire pitch lengths. Figure 18 shows the vector plots of the swirl velocity component in the cross-section planes. The swirl velocity could reach the 30 % of the average velocity in the cross-section u_{sc} (Table 6), and it is highly asymmetric: negligible in the inner sub-channels and strong in the corner and edge sub-channels with a magnitude strongly influenced by the wire position.

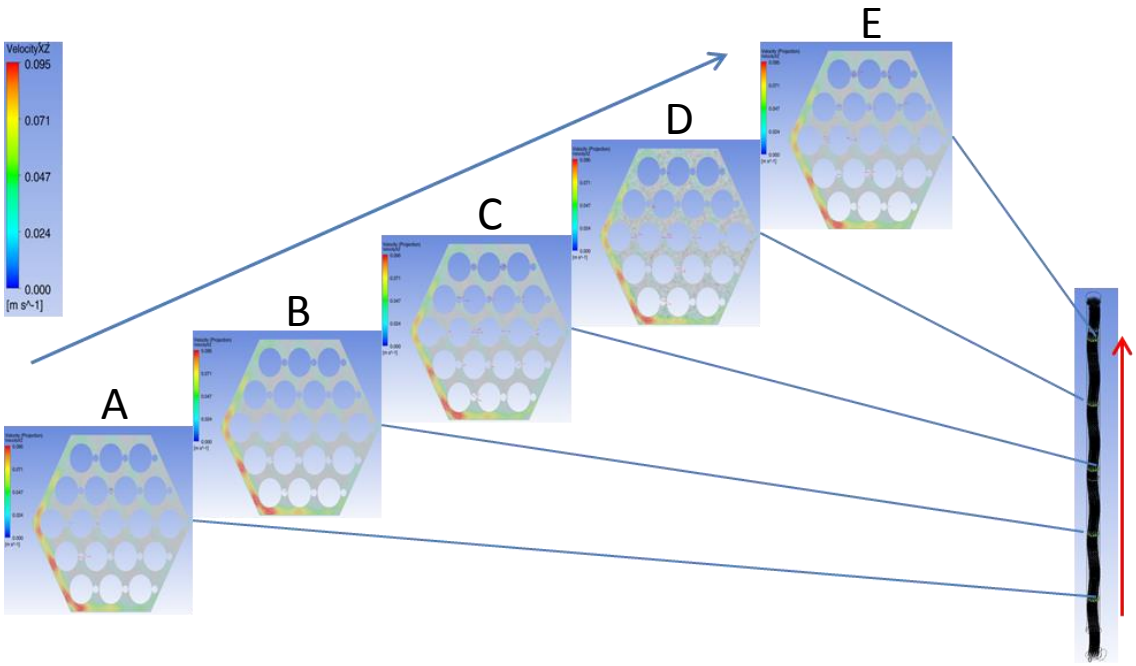

Figure 18 Development of the swirl velocity component for the 2.032 kg/s case.

Looking at the temperature contours (T_{abs}= T - T_{bulk}) on the three different planes of the heated region (Figure 18), it was found that the temperature field is not fully developed. The same results on the temperature field can be deduced from Figure 19, where it is plotted a comparison between the average pin temperature and bulk temperature functions into the heated region obtained by post-processing results of the OF20 case and the SS20 case; it can

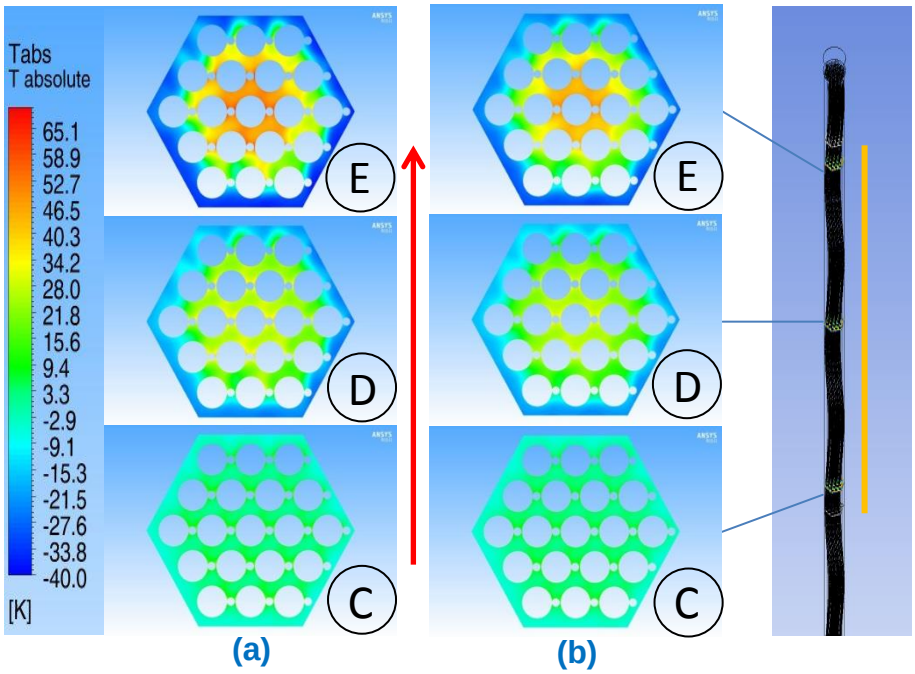

Figure 17 Contours of the Tabs on planes C, D and E in the heated zone (in orange) for the OF20 case (a) and SS20 case (b).

be observed that the average pins temperature and the bulk temperature functions have different slopes either for the complete model case (SS20); the conjugate heat transfer effect is also detected because the average pins temperature for the SS20 case attains lower values and it has a lower slope than the OF20 one.

On the left side of Figure 19 the pressure drop behavior against the vertical coordinate is also reported. The following main features can be evidenced: a singular pressure loss in the entry/developing region (where a sudden constriction is present), a linear slope in the heated and follower regions (another evidence of the fully developed velocity field in the model) and the sudden pressure loss due to the holding grid.

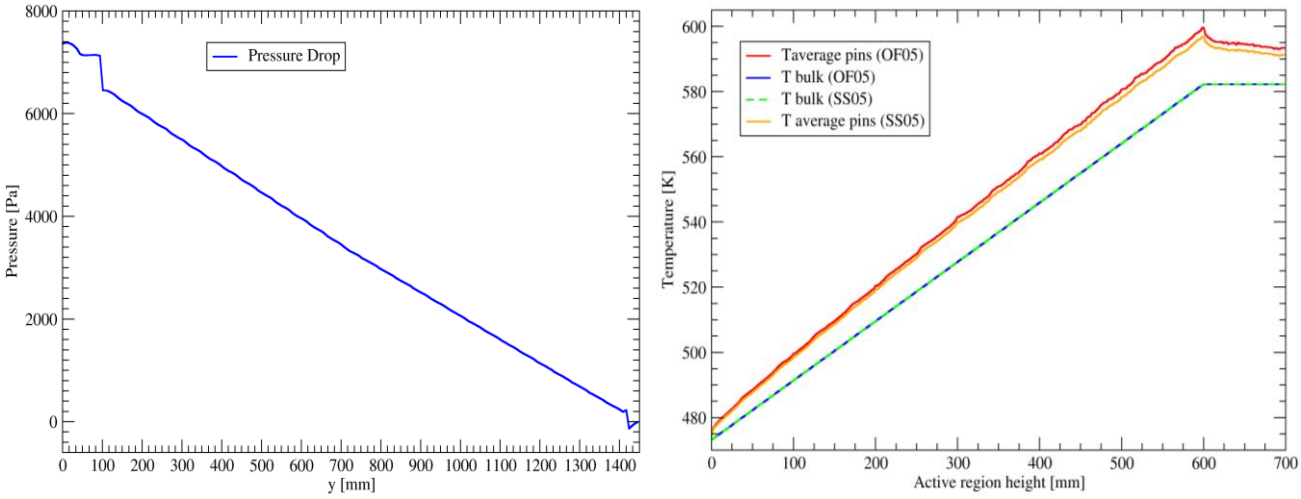

Figure 19 For the 2.032 kg/s case: (right) Bulk temperature and pin average temperature for the SS20 and OF20 cases as function of the height from the heated region inlet plane; (left) Pressure drop against vertical coordinate

6.1. Overall pressure drop

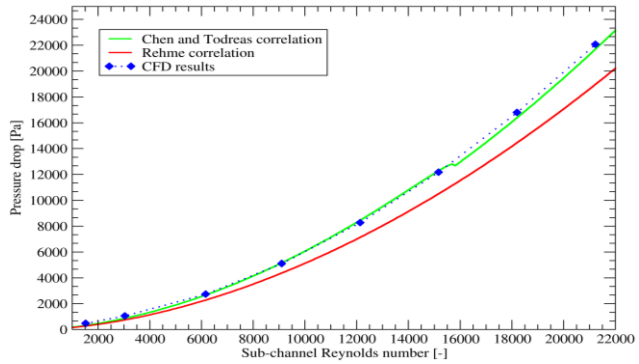

Figure 20 Comparison between the CFD results and the available correlations for the pressure drop in the active region

In addition to the previous results, the present model predictions for a fuel pin bundle with wire spacer using liquid LBE coolant were compared with correlations reported in the open literature. Results of Rehme [16] and Chen and Todreas [17] were chosen for this comparison among reported correlations. The two correlations were chosen because they are considered the most reliable for our bundle geometry. Moreover, the Rehme correlation is the most used in design applications thanks to its simplicity, while the Chen and Todreas correlation is the most precise due to the considerable amount of data used.

The results compared are the pressure drop predictions in the active region of the bundle for the different mass flow rates (i.e. different Reynolds numbers).

Figure 20 shows the pressure drop against the sub-channel Reynolds number from CFD results and from the correlations. CFD results are really in good agreement with the Chen and

Todreas correlation, while Rehme's predictions underestimate the pressure drop. The behavior of the two correlations with respect to the numerical results is perfectly in accordance with the literature with a systematic under-estimation of the Rehme correlation in the whole range.

6.2. The heat transfer issue

During the detailed investigation of the test matrix, it was pointed out that the thermal field is not fully developed in any case investigated. This fact precludes any comparison of our results with the available heat transfer correlations from the literature.
Looking for a better study of the heat transfer phenomena involved into the pin bundle, a new CFD model was developed for studying the heated bundle in fully developed conditions of velocity and temperature.

6.3. The wire pitch model

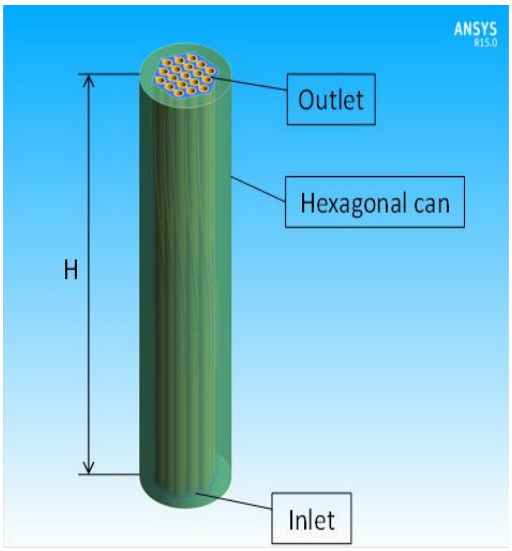

Figure 21 Wire pitch CFD model

The new model developed can be seen as a portion of the complete model; in fact it has the same radial bundle dimensions of the complete model but a total length equal to one wire pitch (262 mm); the solid structures of the 19 pins and wires (in **orange**) and the hexagonal pipe (in **green**) are included (Figure 21).
The mesh elements and the mesh size for the solid and fluid bodies are of the same order of the complete model and similar considerations yield.
The heat flux (*q"*) is imposed on the inner surface of the pins, while the total thermal power is scaled with the model dimensions, the external surface of the hexagonal pipe is imposed adiabatic.
A periodic boundary condition is imposed on the inlet and outlet surfaces of the fluid model for achieving the fully developed conditions of velocity and temperature.
Specific source terms in the Navier-Stokes equations were added in order to achieve a periodic solution. In particular, in the momentum equation

$$\frac{\delta}{\delta t}(\rho\vec{v}) = \nabla\cdot(\rho\vec{v}\vec{v}) = -\nabla p + \nabla(\bar{\bar{\tau}}) + \rho\vec{g} + \vec{F} \qquad (1)$$

The $\vec{F}$ source term

$$\vec{F} = \begin{bmatrix} 0 \\ \frac{\Delta p_{active}}{L_{active}} \\ 0 \end{bmatrix} \qquad (2)$$

was added; where Δp_{active} is the absolute value of the pressure drop into the heated / active region resulting from the complete model case. The $\vec{F}$ term was added in the equation as a

positive pressure head. The mass flow rate through the domain is a result of the calculation. This method practically imposes the value of the average friction factor in the domain.

The energy equation is expressed as :

$$\frac{\delta}{\delta t}(\rho h) + \nabla \cdot (\rho \vec{v} h) = \nabla \cdot \left(k_{eff} \nabla T\right) + \phi' + S_h \quad (3)$$

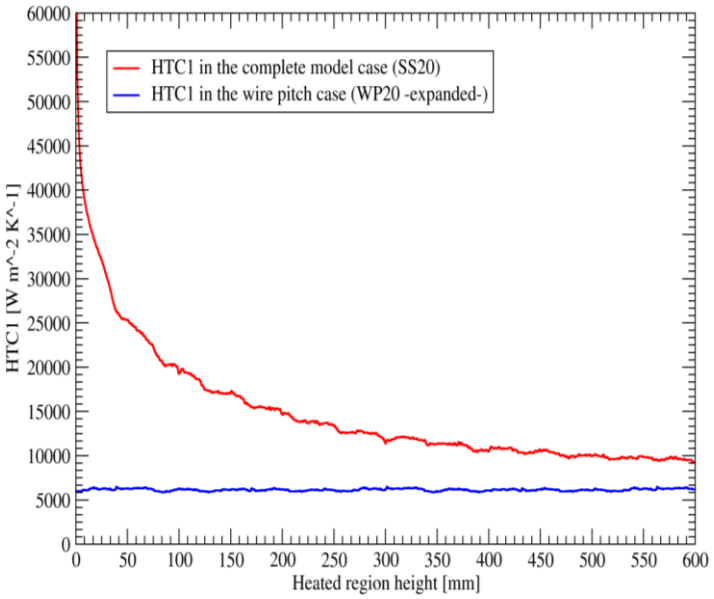

Figure 22 Comparison between the cross-section average HTC in the wire pitch model and in the complete model for

Where h is the specific enthalpy of the fluid, k_{eff} is the effective conductivity ($k + k_t$, where k_t is the turbulent thermal conductivity, defined according to the turbulence model being used). On the left hand side, the terms represent the inertia and the convective transport; on the right hand side the first term is the diffusion of heat and ϕ' is the dissipation function that is generally negligible for incompressible flows. S_h is the volumetric heat source/sink, that in the specific case is defined as

$$S_h = -\frac{W \cdot v_y}{V_{fluid} \cdot \overline{u}_{sc}} \quad (4)$$

where W is the total thermal power given to the fluid, V_{fluid} is the LBE fluid volume and v_y is the stream-wise component of the velocity vector. It has to be noticed that S_h is not a constant term as $\vec{F}$ but it is weighted with the local specific mass flow. Term (4) guarantees the global energy balance within the domain, ensuring the possibility of a periodic solution for temperature. The shape of the source term distribution (4), proportional to the local streamwise velocity, perfectly recovers the physics of heat transfer.

The basic solver options like the convective scheme or the turbulence model are the same of the complete model.

The same numerical test matrix of the complete model was implemented; it has to be noticed that the pressure head implemented in the wire pitch model simulations (Δp_{active}) is the absolute value of the pressure drop calculated in the heated region for the complete model cases simulated (SSXX).

The temperature distributions obtained in the wire wrap model cases are compared with the corresponding results of the complete model. For a correct study of the local heat transfer on a specific section of the fluid, two variables were defined: T_{wall} is the average value of the temperature on the pins at the cross-section height; T_{bulk} is the mass flow average temperature (or mixing cup temperature) of the fluid on a specific cross-section.

A global heat transfer coefficient (HTC_1) on the cross-section was defined as:

$$HTC_1 = \frac{q''}{(T_{wall} - T_{bulk})} \quad (5)$$

It has to be specified that the average pin temperature T_{wall} is calculated only with the temperatures of the rods surfaces. The heat flux (q'') is the same for the two models and varies with the test matrix case only.

The first comparison between the wire pitch model and the complete model is on the cross-section average HTC_1, Equation (5). In Figure 22 HTC_1 for SS20 and WP20 are reported against the heated height. For the complete model (SS20) HTC_1 is calculated at different heights from the inlet section of the heated region, while for the wire pitch model (WP20) the HTC_1 is calculated at different heights of the wire pitch length and its slope repeated and translated for reproducing the heated length geometry.

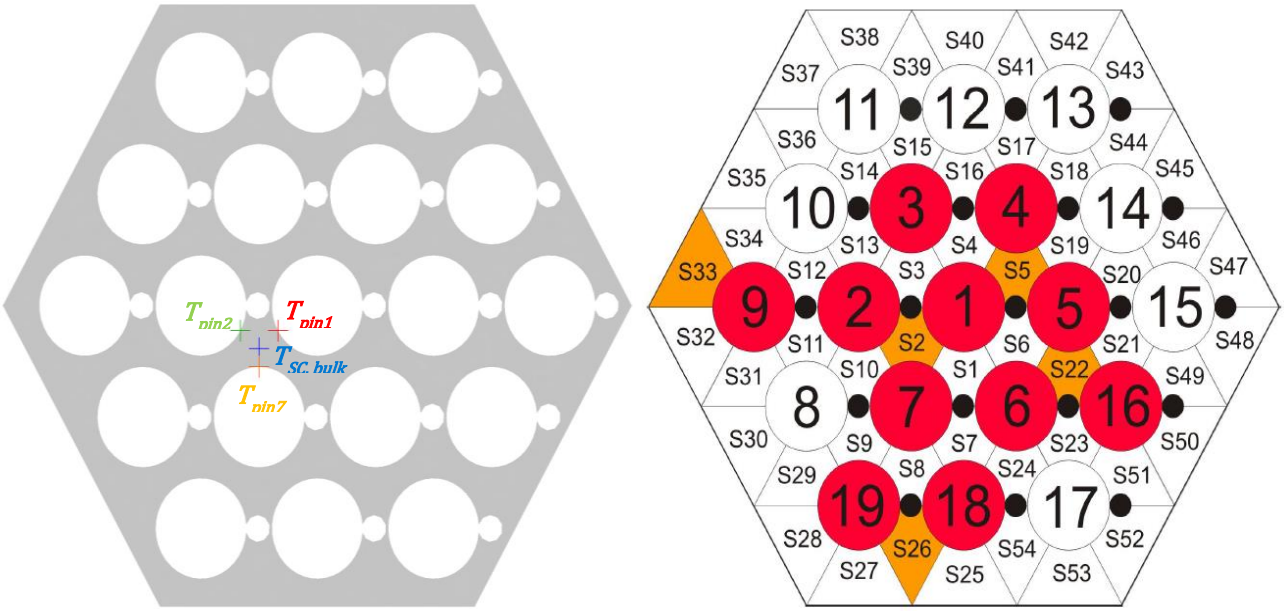

Figure 23 Representation of the measuring points on the inlet plane of the wire pitch model (left) and graphic representation of the instrumented pins and sub-channels into the ERS

HTC_1 in the heated region is not developed but classically tends to its asymptotic value thermal field. Keeping into account that the equivalent diameter is around 4 mm, hundreds of diameters are necessary to reach the asymptotic condition [18]. The same comparison was carried out for the whole test matrix.

The HTC_1 values were not compared with the available heat transfer correlations from the literature because the numerical correlations are based on experimental results that cannot measure the average pin temperature (T_{wall}) but only some thermocouples values on different pins. Moreover the Nu_1 ($Nu_1 = \frac{HTC_1 D_{eq}}{k}$) values resulting from the CFD simulations would be lower than the correlation values because the colder regions in the edge and corner sub-channels drop the average pin temperature and Nu_1. This is especially true for heavy liquid metals where a large thermal boundary layer exist.

For a correct comparison with the available correlations, a new definition of the heat transfer coefficient and Nusselt number must be used.

Experimental-like definitions of HTC and Nusselt number must be based on the local wall temperature and on the channel-center temperature. In this way the comparison with the correlations is more appropriate and adequate. The HTC_2 is therefore defined as:

$$HTC_2 = \frac{q''}{(T_{pins} - T_{SC,bulk})} = \frac{q''}{\Delta T} \quad (6)$$

where

$$T_{pins} = \frac{T_{pin1} + T_{pin2} + T_{pin7}}{3} \quad (7)$$

and $T_{SC,bulk}$ is the temperature measured in the bulk thermocouple position at the center of the S2 sub-channel. On the left side of Figure 23, the measuring points of the CFD models are reported on the inlet plane of the wire pitch model, while on the right side the instrumented pins (in red) and the instrumented sub-channels (in orange) are depicted. For the Nu_2 calculation, the equivalent diameter adopted in the formula is the sub-channel equivalent diameter ($D_{SC,eq}$) of S2 in Figure 23:

$$D_{SC,eq} = \frac{4 \cdot A_{S_2}}{P_{S_2,wet}} = 3.84\ mm \quad (8)$$

where A_{S2} is the flow area of the sub-channel S2 and $P_{S2,wet}$ is the wetted perimeter of the same sub-channel.

A simple representation of the results is shown graphically in Figure 24, where all the results obtained were compared with the Ushakov [19]and Mikityuk [20] heat transfer correlations .

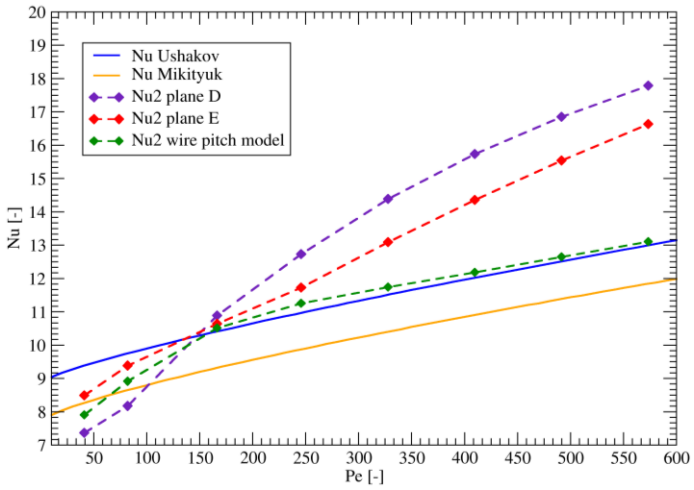

Figure 24 Nu_2 values calculated for the numerical test matrix against the Peclet number compared with the Ushakov correlation and Mikitvuk correlation

Figure 24 shows that the thermal field is not fully developed in the complete model: the Nu_2 values tend to decrease to the asymptotic trend of the wire pitch model results for mass flow rates higher than 2 kg/s. In the same graph are also reported two best fitting heat transfer correlations (the Ushakov and the Mikityuk ones) : the asymptotic values found are anyway higher than the predictions of the Ushakov correlation but tend to its value at higher mass flow rates. Nevertheless, it must be underlined that there are not correlations specifically developed for wire-wrap bundle geometry with heavy liquid metals, and the two correlations adopted basically refer to grid spaced LM cooled bundles. The wire wrap geometry tends to increase the heat transfer because of the swirl flow and the increased turbulence level.

The lower mass flow rate cases simulated (SS05 and SS10 cases) show a rather different behavior of the Nusselt number; the values calculated for the complete model simulations, in facts, are higher than the asymptotic ones of the wire pitch model simulations but anyway more similar to the correlation predictions; the asymptotic Nusselt number values of the wire pitch cases are lower than the Ushakov prediction but anyway near the Mikityuk values.

7. Comparison with experimental data

In this section, a comparison with an experimental test case is provided. The case is named P223 and it is part of the experimental test matrix of the FP7 SEARCH project. The flow and power data of the test case are reported in Table 6. The specific method to measure the mass flow rate the way to post-process data is fully described in [21] and it is currently under publication; the error analysis was performed as well and the error propagation theory was applied for the derived quantities.

Table 6 Power and flow data for P223 experimental test case.

Case	$\dot{m}_{NACIE}$ [kg/s]	Thermal power [kW]	T_{in}[°C]
P223	3.40	52	250

Figure 25 shows the experimental vs numerical bulk temperatures for case P223 in all the bulk thermocouples of the test section. The agreement is relatively good except from some values in section C.

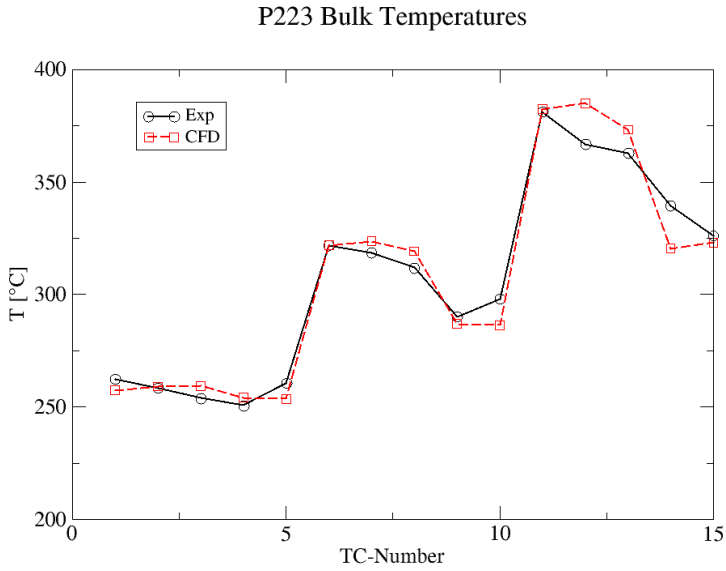

Figure 25 Experimental vs. numerical Bulk temperatures for case P223.

Figure 26 shoes the axial temperature distribution along the pin n.3 for the wall thermocouples compared with the CFD monitoring points in the same position. The agreement is good and the both the temperature values and the mean slope are well captured.

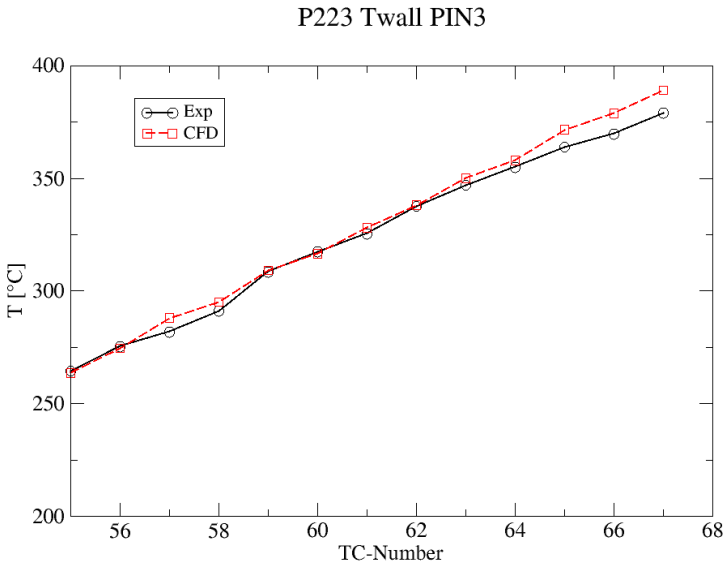

Figure 26 Experimental vs. numerical axial wall temperature distribution along the axis.

Figure 27 the local Nusselt number is the intermediate, central section B post-processed from the experimental data and by numerical CFD simulation. Values in subchannels S5, S22 and S26 are very well captured and the spatial distributions of the local Nusselt with a minimum in S26 is also well captured.

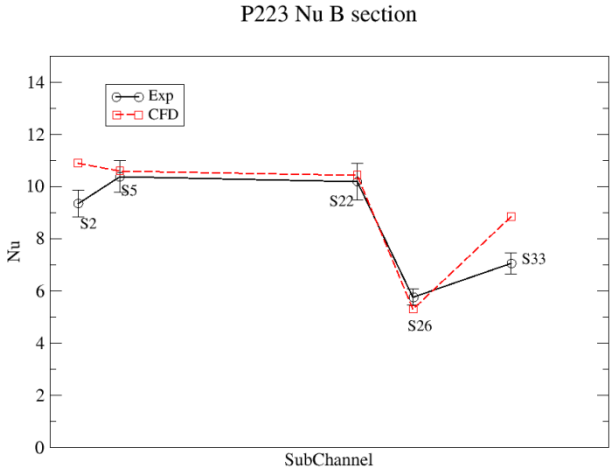

Figure 27 Experimental vs. numerical local Nusselt number in the intermediate section B.

8. Conclusions

A CFD pre-test analysis was carried out on the NACIE-UP fuel pin bundle simulator (FPS) placed at the ENEA Brasimone Research Centre. The FPS has 19-pins, it is wire-wrapped and

it is cooled with liquid Lead Bismuth Eutectic (LBE) and the study is in the context of GEN.-IV nuclear reactors research.
An experimental campaign will be carried out in 2014 on the bundle coolability in the context of the SEARCH FP7 EU project to support the MYRRHA design. The thesis documents the code assessment for the wire wrap bundle geometry, the CFD model developed to describe the experimental test section, the sensitivity analysis developed on the model, model validations and pre-test results.
The whole FPS test section was modelled including the inlet region, the entry region, the active region, the outlet region with the upper grid, and the hexagonal wrap. The total number of nodes and elements in the model was $3.5 \cdot 10^7$ and $9.7 \cdot 10^7$ respectively, with wall resolution $y^+ = 1 - 4$ in the range of interest. Stationary RANS computations were performed for the whole experimental range with mass flow rates from 0.5 to 7 kg/s and with a corresponding Reynolds number from $1.5 \cdot 10^3$ to $2.1 \cdot 10^4$.
A CFD code validation was carried out on experimental data by ORNL in a similar geometry cooled by sodium. Results showed a global coherence of the results and a correct description of the conjugate heat transfer effects. A good agreement was found between numerical and experimental data, although the RANS approach showed some limitations for the central sub-channel temperature distributions at high mass flow rates.
The velocity field in the wire-wrapped assembly of NACIE-UP shows complex features and a strong secondary fluid flow due to the swirl. Results show that the hydrodynamic field is well developed well before the beginning of the active region after one wire pitch about. Nevertheless, the thermal field is not fully developed in the active region and the slopes of the wall and bulk temperatures are different. This fact is not new and it was evidenced by other authors [20]. A good agreement was obtained by comparing CFD results with existing pressure drop correlations on wire-wrapped bundles; in particular a very good agreement was obtained with the Chen & Todreas correlation [17]. Moreover, a friction factor oscillation near its mean value was observed in all the test matrix with a constant period equal to 1/6 P_w, imposed by the geometrical constraints.
Regarding the conjugate heat transfer effect, from numerical simulations it is clear that the conduction in the wrap pipe structure and in the wire is very important to correctly capture the temperature gradients, the local temperature maxima close to the wire and temperature minima in the edge sub-channels, especially for the lower Reynolds number cases. The undeveloped thermal field of the test matrix cases simulated, the absence of heat transfer correlations specifically developed for wire wrap pin bundle geometry and the uncertainty in the nomenclature and definitions precluded a structured validation of the results, developing an asymptotic wire pitch domain and adopting different definitions of HTC and Nu for a comparison with the available heat transfer correlations for liquid metal cooled bundles.
Several highlights for the experimental activity emerged by the pre-test CFD analysis. In particular, the fuel bundle power should be increased as much as possible in the low mass flow rate range to improve the accuracy on the heat transfer coefficient measurement. Moreover, the numerical evidence of the not fully developed thermal field in the bundle,

implies that experimental results must be released with details on the experimental test facility and boundary conditions.

The CFD model developed in the present master thesis will be the basis for the post-test CFD analysis of the NACIE-UP FPS test section. In particular, the CFD model will be used in 'stationary way' for all the cases of the experimental test matrix, and in 'transient way' (URANS) for some specific experiments, i.e. the foot flow blockage obtained by partially closing a valve in the primary loop of NACIE-UP. The subsequent assessment of the methodology and of the model by the direct comparison with experimental data will qualify CFD for wire-wrap bundles cooled by heavy liquid metal.

References

[1] H.A. Abderrahima, P. Kupschusa, E. Malambua, Ph. Benoita, K. Van Tichelen, B. Ariena, F. Vermeerscha, P. D'hondta, Y. Jongenb, S. Ternierb, D. Vandeplassche, MYRRHA: A multipurpose accelerator driven system for research & development, Nuclear Instruments and Methods in Physics Research A 463 (2001) 487-494

[2] P. Turroni, L.Cinotti et al., The CIRCE Test Facility, ANS Winter Meeting, Reno ,2001.

[3] I. Di Piazza, P. Gaggini, M. Tarantino, M. Granieri, The fuel rod bundle design for the NACIE facility, ENEA SEARCH project, deliverable (D-N°2.1), 2012.

[4] R. Gajapathy, K. Velusamy, P. Selvaraj, P. Chellapandi, S.C. Chetal, CFD investigation of helical wire-wrapped 7-pin fuel bundle and the challenges in modelling full scale 217 bundle, Nuclear Engineering and Design 237 (2007) 2332–2342.

[5] J. Lafay et al., ASME paper 75-HT-22 ,1975.

[6] T.B. Barholet et al., CRBRP-ARD-0108 , January 1977.

[7] T.G. Bartholet et al., WARD-D-0161 ,October 1976.

[8] N. Todreas, Personal communications, MIT, to A.A. Bishop, 1979.

[9] R. Gajapathy, K. Velusamy, P. Selvaraj, P. Chellapandi, S.C. Chetal, CFD investigation of helical wire-wrapped 7-pin fuel bundle and the challenges in modelling full scale 217 bundle, Nuclear Engineering and Design 237 (2007) 2332–2342.

[10] R. Gajapathy, K. Velusamy, P. Selvaraj, P. Chellapandi, S.C. Chetal, A comparative CFD investigation of helical wire-wrapped 7, 19 and 37 fuel pin bundles and its extendibility to 217 pin bundle, Nuclear Engineering and Design 239 (2009) 2279–2292.

[11] M.H. Fontana, Temperature Distribution in the Duct Wall and at the Exit of a 19-Rod Simulated LMFBR Fuel Assembly (FFM-2A), ORNL-4852, Oak Ridge National Laboratory ,1973.

[12] ANSYS CFX Release 15 User Manual.

[13] F.R. Menter, Two-equation eddy-viscosity turbulence models for engineering applications, AIAA J 32 (1994) 269-289.

[14] X. Cheng, N.I. Tak, CFD analysis of thermal-hydraulic behavior of heavy liquid metals in sub-channels, Nuclear Engineering and Design 236 (2006) 1874-1885.

[15] OECD/NEA, Handbook on Lead-bismuth Eutectic Alloy and Lead Properties Materials Compatibility Thermal-hydraulics and Technologies, NEA 6195, 2007.

[16] K. Rehme, Pressure drop correlations for fuel element spacers. Nuclear Technology 17 (1973) 15–23.

[17] S.K. Cheng, N.E. Todreas, Hydrodynamic models and correlations for bare and wire-wrapped hexagonal rod bundles - bundle friction factors, sub-channel friction factors and mixing parameters, Nuclear Engineering and Design 92 (1986) 227–251.

[18] N.G. Rasu, K. Velusamy, T. Sundararajan, P. Chellapandi, Simultaneous development of flow and temperature fields in wire-wrapped fuel pin bundles of sodium cooled fast reactor, Nuclear Engineering and Design 267 (2014) 44-60.

[19] P.A. Ushakov, A.V. Zhukov and M.M. Matyukhin, Heat transfer to liquid metals in regular arrays of fuel elements, High Temperature 15 (1977) 868–873; translated from Teplofizika Vysokikh Temperatur 15 (5) 1027–1033.

[20] K. Mikityuk, Heat transfer to liquid metal: Review of data and correlations for tube bundles, Nuclear Engineering and Design 239 (2009) 680–687.

[21] I. Di Piazza, M. Angelucci, R. Marinari, M. Tarantino, N. Forgione, Heat Transfer On Hlm Cooled Wire-Spaced Fuel Pin Bundle Simulator In The Nacie-Up Facility, submitted to Nucl. Eng. Des., 2015.